Check for updates

ADVANCED MATERIALS
www.advmat.de

Solution Processed Bilayer Metal Halide White Light Emitting Diodes

*He Liu, Tunde Blessed Shonde, Oluwadara Joshua Olasupo, Tarannuma Ferdous Manny, Md Sazedul Islam, Jarek Viera, Mohammad Khizr, Sahel Moslemi, Xinsong Lin, J.S. Raaj Vellore Winfred, Layla El Nasser, Keyou (Sam) Mao, and Biwu Ma**

Metal halide perovskites and perovskite-related organic metal halide hybrids (OMHHs) have recently emerged as a new class of luminescent materials for light emitting diodes (LEDs), owing to their unique and remarkable properties, including near-unity photoluminescence quantum efficiencies, highly tunable emission colors, and low temperature solution processing. While substantial progress has been made in developing monochromatic LEDs with electroluminescence across blue, green, red, and near-infrared regions, achieving highly efficient and stable white electroluminescence from a single LED remains a challenging and under-explored area. Here, a facile approach to generating white electroluminescence is reported by combining narrow sky-blue emission from metal halide perovskites and broadband orange/red emission from zero-dimensional (0D) OMHHs. For the proof of concept, utilizing $TPPcarz^+$ passivated two-dimensional (2D) $CsPbBr_3$ nanoplatelets (NPLs) as sky blue emitter and 0D $TPPcarzSbBr_4$ as orange/red emitter ($TPPcarz^+$ = triphenyl (9-phenyl-9H-carbazol-3-yl) phosphonium), white LEDs (WLEDs) with a solution processed bilayer structure have been fabricated to exhibit a peak external quantum efficiency (EQE) of 4.8% and luminance of 1507 cd m^{-2} at the Commission Internationale de L'Eclairage (CIE) coordinate of (0.32, 0.35). This work opens a new pathway for creating highly efficient and stable WLEDs using metal halide perovskites and related materials.

1. Introduction

White light emitting diodes (WLEDs) have changed the modern world over the last decades with wide applications in full color displays and solid-state lighting.[1] However, most practical WLEDs are optically pumped ones consisting of blue LED (e.g., InGaN) chips and rare-earth based inorganic phosphors with limited utility, energy, and cost efficiency.[2] Electrically driven WLEDs are highly desirable to resolve the environmental and efficiency concerns of optically pumped WLEDs.[3] However, electrically driven WLEDs based on either inorganic semiconductors or organic semiconductors developed to date still face serious issues and challenges with high costs in both materials and device manufacturing.[4] Developing WLEDs with low cost materials and facile fabrication processes is of great scientific and practical importance.[5]

Recently, metal halide perovskites and perovskite-related hybrid materials have received great research attention as new generation luminescent materials for LEDs, due to their highly tunable and efficient emissions, excellent charge transport properties, and low temperature processing.[6] While remarkable progress has been achieved in the development of monochromatic LEDs with emissions covering blue to green, red, and near-infrared regions, obtaining efficient and stable WLEDs based on these materials remains highly challenging.[7] WLEDs utilizing white-emitting layers made from mixtures of red, green, and blue perovskite emitters experience several issues, such as ion exchange and energy transfer among different emission centers, along with difficulties in film processing.[8] To address these issues, researchers have adopted a tandem structure by inserting intermediate connection layers between different perovskite emitting layers for multilayered WLEDs.[9] However, the creation of additional interfaces with voltage drops across interlayers results in electroluminescence discrepancies between different emitting layers and reduced performance.[10] Combining organic and perovskite emitters for hybrid WLEDs has also been demonstrated in several studies.[11] However, these devices suffer from unbalanced charge carrier recombination, shifting exciton formation zones under different applied voltages, and undesired energy transfer between emitters.[12] Therefore, it is crucial to develop effective strategies to address these issues in WLEDs based on metal halide perovskites and related materials.

H. Liu, T. B. Shonde, O. J. Olasupo, T. F. Manny, M. S. Islam, J. Viera, M. Khizr, S. Moslemi, X. Lin, J. R. V. Winfred, L. E. Nasser, B. Ma
Department of Chemistry and Biochemistry
Florida State University
Tallahassee, FL 32306, USA
E-mail: bma@fsu.edu
K. (Sam) Mao
Magnet Science and Technology
National High Magnetic Field Laboratory
Tallahassee, FL 32310, USA

The ORCID identification number(s) for the author(s) of this article can be found under https://doi.org/10.1002/adma.202412239

DOI: 10.1002/adma.202412239

 © 2024 Wiley-VCH GmbH

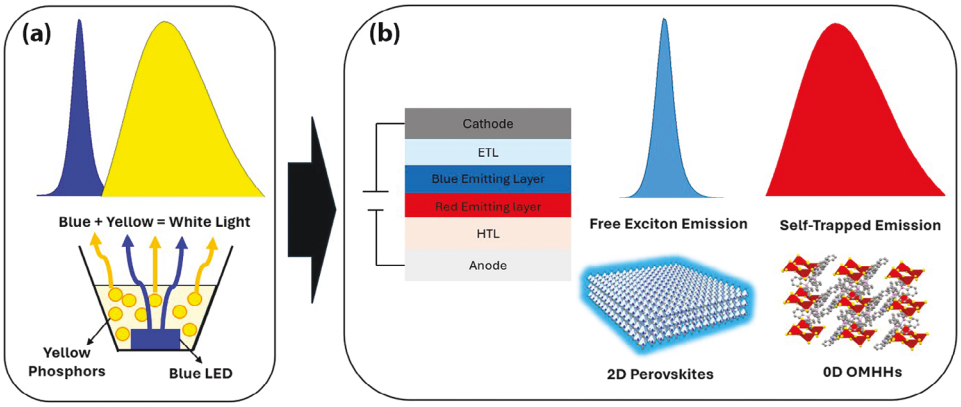

Figure 1. a) Schematics of a typical WLED consisting of a blue LED and yellow phosphors. b) The design concept of achieving white electroluminescence by combining narrow band free exciton and broadband self-trapped exciton emissions.

Here we report a new method for generating white electroluminescence by combining narrow sky-blue emission from metal halide perovskites and broadband orange/red emission from perovskite-related zero-dimensional (0D) organic metal halide hybrids (OMHHs). Specifically, by utilizing $TPPcarz^+$ passivated two-dimensional (2D) $CsPbBr_3$ nanoplatelets (NPLs) as the sky-blue emitter and 0D $TPPcarzSbBr_4$ as the orange/red emitter ($TPPcarz^+$ = triphenyl (9-phenyl-9H-carbazol-3-yl) phosphonium), WLEDs have been fabricated to exhibit a peak external quantum efficiency (EQE) of 4.8% and luminance of 1507 cd m^{-2} at the CIE coordinate of (0.32, 0.35). Due to the distinct solubility properties of surface passivated 2D $CsPbBr_3$ NPLs and 0D $TPPcarzSbBr_4$, a bilayer structure with 2D $CsPbBr_3$ NPLs on top of 0D $TPPcarzSbBr_4$ can be obtained via facile solution processing using orthogonal solvents, i.e., dimethylformamide (DMF) for 0D $TPPcarzSbBr_4$ and n-octane for 2D $CsPbBr_3$ NPLs. Unlike most bilayer WLEDs that exhibit energy transfer between two emitting layers, our WLEDs do not experience energy transfer because there is no spectral overlap between the emission of 2D $CsPbBr_3$ NPLs and the absorption of 0D $TPPcarzSbBr_4$. Additionally, the presence of the same organic cation ($TPPcarz^+$) in surface passivated 2D $CsPbBr_3$ NPLs and 0D $TPPcarzSbBr_4$ ensures efficient charge transport across the bilayer structure, minimizing energy loss in two directly connected emitting layers.

2. Results and Discussion

One common method to achieve white emission involves combining narrow blue emission with broadband yellow or orange/red emission. This approach is often seen in commercially available WLEDs, which consist of blue LED chips paired with down-conversion rare-earth-based inorganic phosphors (**Figure 1a**).[13] Here we have attempted to achieve white emission using a similar strategy: combining narrow blue emission with broadband yellow or orange/red emission.[14] However, unlike the traditional approach where one emission is electroluminescent and the other is photoluminescent, both emissions in this work are electroluminescent.[15] The design concept of our WLEDs is illustrated in Figure 1b, which consist of a stack of sky blue emitting layer made of 2D perovskites with direct band free-exciton emission and orange/red emitting layer made of 0D OMHHs with strongly stokes shifted broadband self-trapped emission.[16] Based on our previous studies on monochromatic LEDs,[17] we have chosen $TPPcarz^+$ passivated 2D $CsPbBr_3$ NPLs as blue emitter and 0D $TPPcarzSbBr_4$ as orange/red emitter. The major rationales behind our strategy are multifaceted: i) the lack of spectral overlap between the emission of 2D $CsPbBr_3$ NPLs and the absorption of 0D $TPPcarzSbBr_4$ minimizing energy transfer between two emitting layers, ii) the presence of the same semiconducting organic cation ($TPPcarz^+$) in both 2D $CsPbBr_3$ NPLs and 0D $TPPcarzSbBr_4$ providing good energy level alignment to facilitate charge transport, and iii) the feasibility of layer-by-layer solution processing using orthogonal solvents.

Before fabricating WLEDs, we first established efficient sky-blue LEDs based on 2D $CsPbBr_3$ NPLs. To achieve better color mixing with orange/red emitters for white emission, we focused on 2D $CsPbBr_3$ NPLs with a sky blue emission peaked at ≈490 nm, instead of pure blue emission peaked at ≈455 nm as reported before.[17b] Following a previously established synthetic protocol, we tuned the reaction temperature and the $TPPcarzSO_4$ and TPPcarzBr molar ratios to oleylamine (see details in Experimental Section)[18] to prepare 2D $CsPbBr_3$ NPLs with a thickness of 5 units of $PbBr_6^{4-}$ octahedra (≈3 nm) and a lateral size of up to 300 nm (**Figure 2a**).[14b,19] The interaction between TPPcarzBr/$TPPcarz_2SO_4$ and the 2D $CsPbBr_3$ layer, as well as the passivation mechanism, has been discussed in our earlier work.[17b] Optical characterizations reveal a sky blue emission peaked at 490 nm with an full width at half maximum (FWHM) of 20 nm from these 2D $CsPbBr_3$ NPLs, as shown in Figure 2b. Solution processed thin films based on these 2D $CsPbBr_3$ NPLs, with a high PLQE of up to 86%, were then used to fabricate sky blue LEDs, with a device structure of ITO/poly (ethylenedioxythiophene): polystyrene sulfonate (PEDOT:PSS)/poly(9-vinylcarbazole) (PVK)/2D $CsPbBr_3$ NPLs/1,3,5-Tris (1-phenyl-1H-benzimidazol-2-yl) benzene (TPBi)/LiF/Al (Inset of Figure 2c). Stable sky-blue electroluminescence (EL) peaked at 490 nm is recorded for these devices and is independent of the operation voltage, as shown in Figure 2c. The device characteristics of a sky-blue LED based on 2D $CsPbBr_3$ NPLs are shown in Figure 2d,e, which exhibits a luminance of 2233 cd m^{-2} at 10 V, an EQE of 10.4%, and a current efficiency of 13.4 cd A^{-1}.

© 2024 Wiley-VCH GmbH

15214095, 2025, 25, Downloaded from https://advanced.onlinelibrary.wiley.com/doi/10.1002/adma.202412239 by Biwu Ma - Florida State University , Wiley Online Library on [20/12/2025]. See the Terms and Conditions (https://onlinelibrary.wiley.com/terms-and-conditions) on Wiley Online Library for rules of use; OA articles are governed by the applicable Creative Commons License

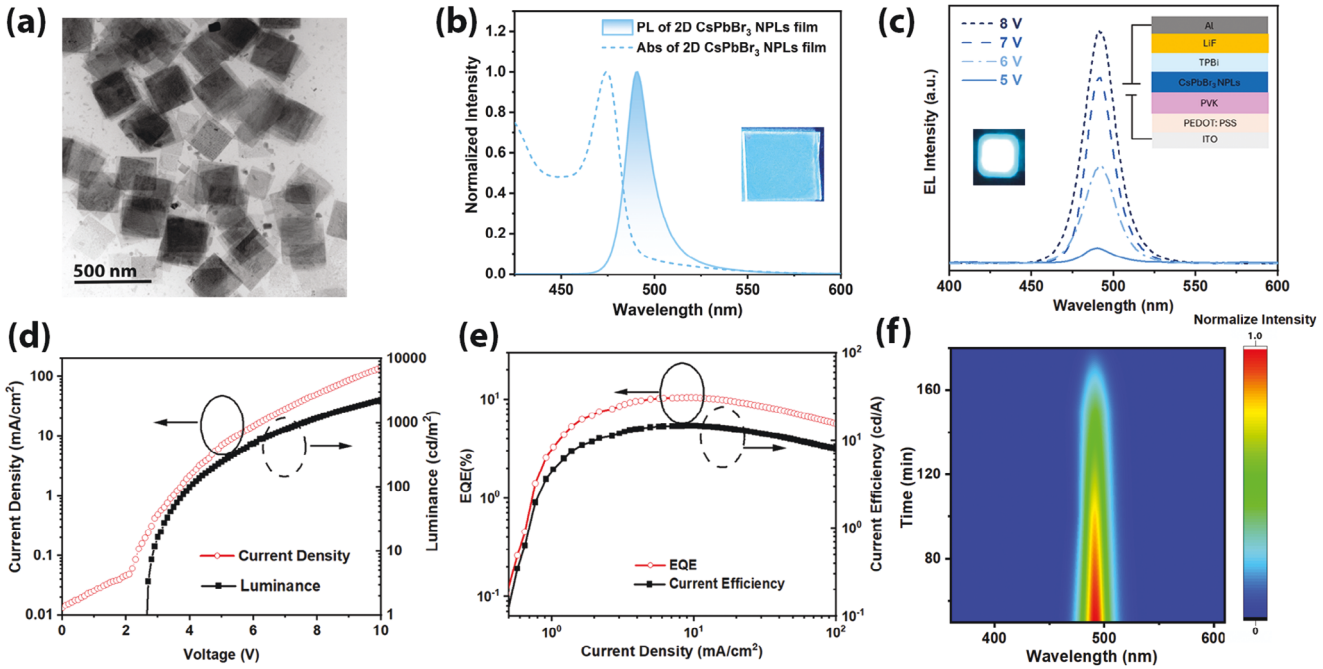

Figure 2. a) TEM image of 2D $CsPbBr_3$ NPLs. b) Absorption and emission spectra of films based on 2D $CsPbBr_3$ NPLs (the inset shows a film under UV 365 nm light). c) EL spectra of devices based on 2D $CsPbBr_3$ NPLs at different operational voltages (the insets show a working device at 5V and the device structure). d) Current density–voltage–luminance and e) EQE–current density–current efficiency diagrams of sky-blue LEDs based on 2D $CsPbBr_3$ NPLs. f) The EL spectra changes with the operational lifetime of sky-blue LEDs based on 2D $CsPbBr_3$ NPLs.

These blue LEDs demonstrate excellent spectral stability during operation, with almost no shift of the emission peak, as shown in Figure 2f. The half lifetime (T_{50}) at an initial luminance of 100 cd m^{-2} is determined to be more than 150 min (Figure S1a, Supporting Information). Moreover, excellent reproducibility is demonstrated by these sky-blue LEDs based on 2D $CsPbBr_3$ NPLs (Figure S1b, Supporting Information).

With the availability of efficient and stable monochromic sky-blue LEDs based on 2D $CsPbBr_3$ NPLs, the next step was to integrate them with orange/red ones to achieve WLEDs. Here we have chosen 0D $TPPcarzSbBr_4$ with an emission peaked at 653 nm and a FWHM of 141 nm to construct an orange/red emitting layer, which have been previously used for the fabrication of LEDs exhibiting an EQE of 5.12%.[17a] A key consideration is the absence of spectral overlap between the emission of 2D $CsPbBr_3$ NPLs and the absorption of 0D $TPPcarzSbBr_4$, which prevents any energy transfer between them. **Figure 3a** shows the absorption and emission spectra of 2D $CsPbBr_3$ NPLs and 0D $TPPcarzSbBr_4$. With an extremely large Stokes shift, 0D $TPPcarzSbBr_4$ has no light absorption in the region of 380–550 nm, meaning that the sky-blue emission from 2D $CsPbBr_3$ NPLs will not be absorbed by 0D $TPPcarzSbBr_4$. As a result, no resonance energy transfer will occur from 2D $CsPbBr_3$ NPLs to 0D $TPPcarzSbBr_4$ when they are stacked together.[20]

To prepare a bilayer of 0D $TPPcarzSbBr_4$/2D $CsPbBr_3$ NPLs, we have taken advantage of the solvent orthogonality during the solution processing of the two layers. As previously reported, 0D $TPPcarzSbBr_4$ thin films can be prepared by spin coating a $TPPcarzSbBr_4$ precursor solution in DMF, while thin films based on 2D $CsPbBr_3$ NPLs can be solution processed in non-polar n-octane. Here we have produced 0D $TPPcarzSbBr_4$ layer as the bottom layer using DMF followed by the deposition of pre-prepared 2D $CsPbBr_3$ NPLs on the top using n-octane. The PLQE of the bilayer emitting layer was measured to be 79.3%, as shown in the spectral curve in Figure S2 (Supporting Information). Figure 3b shows photo images (under UV light) and atomic force microscopy (AFM) images of solution processed 0D $TPPcarzSbBr_4$ layer (40 nm) and 0D $TPPcarzSbBr_4$/2D $CsPbBr_3$ NPLs bilayer stack (110 nm), which exhibit orange/red and white emissions, respectively. The solution processed thin films exhibit excellent uniformity and smoothness, with root mean square roughness measured at 0.04 nm for the 0D $TPPcarzSbBr_4$ layer and 0.159 nm for the stacked bilayer of 0D $TPPcarzSbBr_4$/2D $CsPbBr_3$. SEM images further confirmed the formation of uniform and smooth thin films via simple solution processing (Figure S3, Supporting Information). The successful preparation of high-quality stacked bilayer thin films is attributed to the use of orthogonal solvents and the presence of $TPPcarz^+$ units in both 0D $TPPcarzSbBr_4$ and 2D $CsPbBr_3$ NPLs, which ensures good miscibility.[21] To assess the environmental stability of the emitting layer, we measured the photoluminescence spectra of 0D $TPPcarzSbBr_4$/2D $CsPbBr_3$ NPLs bilayer thin films over 7 days in ambient conditions. As shown in Figure S4 (Supporting Information), the emission spectra show negligible shifts in peak positions, with the PL intensity retaining more than 90% of its initial value after 7 days of storage under ambient conditions.

To experimentally reveal that the emission of 2D $CsPbBr_3$ NPLs is not quenched by 0D $TPPcarzSbBr_4$ in solution processed bilayer structured films, we have performed photophysical studies using steady state and time resolved fluorescence

© 2024 Wiley-VCH GmbH

15214095, 2025, 25, Downloaded from https://advanced.onlinelibrary.wiley.com/doi/10.1002/adma.202412239 by Biwu Ma - Florida State University , Wiley Online Library on [20/12/2025]. See the Terms and Conditions (https://onlinelibrary.wiley.com/terms-and-conditions) on Wiley Online Library for rules of use; OA articles are governed by the applicable Creative Commons License

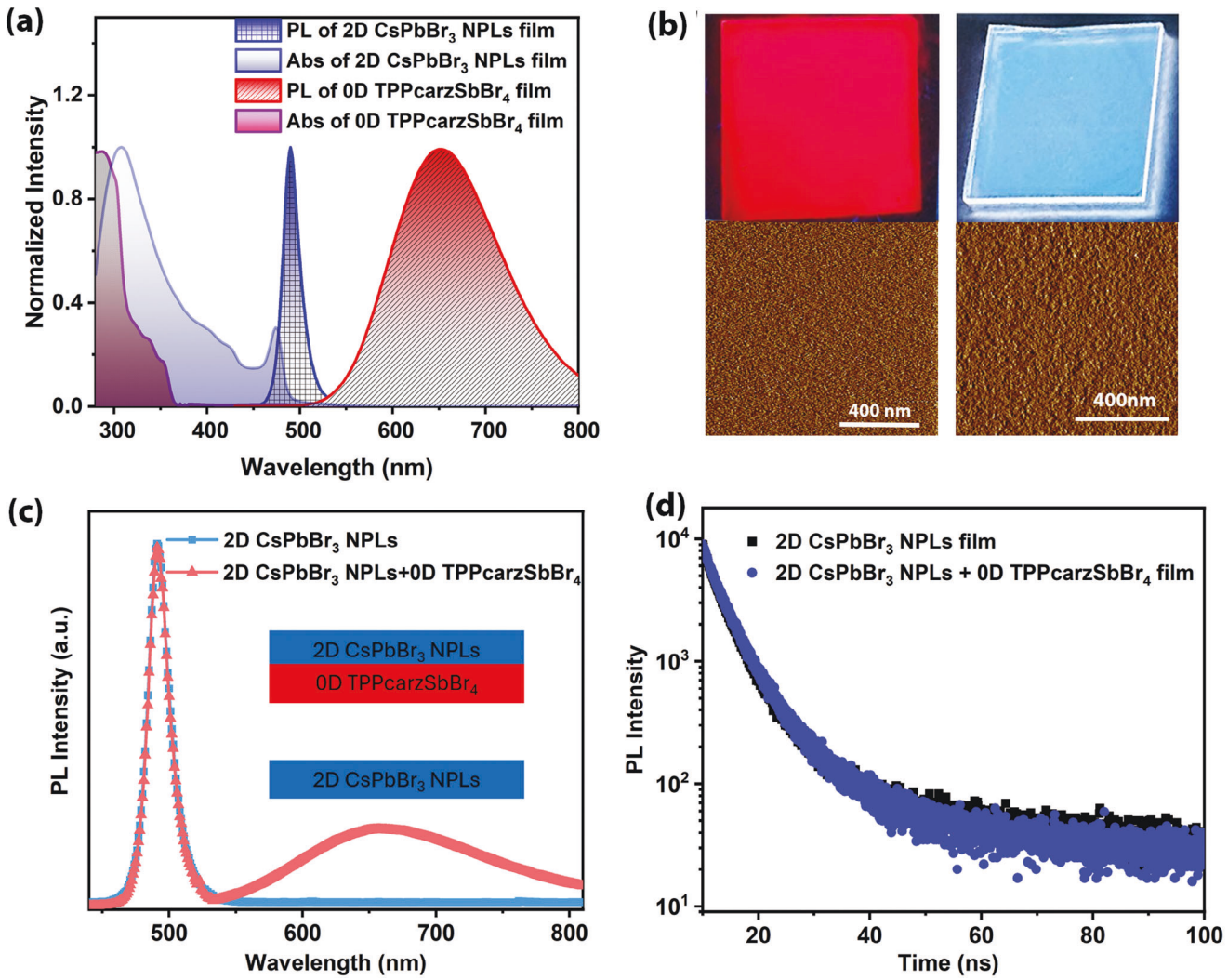

Figure 3. a) Absorption and emission spectra of individual 2D $CsPbBr_3$ NPL thin film and 0D $TPPcarzSbBr_4$ thin film. b) Photos and AFM images of 0D $TPPcarzSbBr_4$ thin film and 2D $CsPbBr_3$ NPLs stacked $TPPcarzSbBr_4$ bilayer thin film. c) Emission spectra of 2D $CsPbBr_3$ NPL thin film and 2D $CsPbBr_3$ NPL stacked 0D $TPPcarzSbBr_4$ bilayer thin film. d) Decay lifetimes of 2D $CsPbBr_3$ NPL thin film with and without 0D $TPPcarzSbBr_4$ layer attached to.

spectroscopies. Figure 3c shows the emission spectra of a thin film based on 2D $CsPbBr_3$ NPLs (40 nm) and a bilayer film of 0D $TPPcarzSbBr_4$/2D $CsPbBr_3$ NPLs (110 nm). It is found that the emission of 2D $CsPbBr_3$ NPLs peaked at 490 nm does not change before and after it being stacked with 0D $TPPcarzSbBr_4$, clearly suggesting there is no energy transfer from 2D $CsPbBr_3$ NPLs to 0D $TPPcarzSbBr_4$. Figure 3d shows the time-resolved PL decay curves of 2D $CsPbBr_3$ NPLs and bilayer thin film samples, which are almost identical with the decay lifetimes determined to be ≈3 ns, further confirming no quenching of the emission of 2D $CsPbBr_3$ NPLs by 0D $TPPCarzSbBr_4$ due to no spectral overlap.[22]

With bilayer 0D $TPPcarzSbBr_4$/2D $CsPbBr_3$ NPLs thin films available, we have fabricated LEDs using a device structure of ITO/PEDOT: PSS (40 nm)/PVK (35 nm)/0D $TPPcarzSbBr_4$ (40 nm)/2D $CsPbBr_3$ NPLs (70 nm)/TPBi (40 nm)/LiF (2 nm)/Al (100 nm). The thicknesses of 0D $TPPcarzSbBr_4$ and 2D $CsPbBr_3$ NPLs layers can be well controlled to achieve emissions with different colors. **Figure** 4a shows the electroluminescence spectra of a device containing an emitting bilayer of 0D $TPPcarzSbBr_4$ (40 nm)/2D $CsPbBr_3$ NPLs (70 nm). The device exhibits white emission with a color temperature of ≈6 000 K and minimum shifts of CIE coordinates across the operating biases from 4 to 7 V, as shown in Figure 4a. This result suggests that the carrier recombination region remains almost unaffected by the driving voltages, which is mainly attributed to the similar charge carrier mobilities of two layers and good energy alignment. We measured the space-charge-limited currents (SCLCs) for thin films based on 2D $CsPbBr_3$ NPLs (Figure S5, Supporting Information),[23] from which hole and electron mobilities of 6.2 × 10^{-6} and 8.1 × 10^{-6} cm^2 V^{-1} s^{-1} were determined, which are in the same order of magnitude as those of thin films based on $TPPcarzSbBr_4$ (hole and electron mobilities of 1.3× 10^{-6} and 3.2×10^{-6} cm^2 $V^{-1}s^{-1}$).[17a]

We further investigated the balanced charge and carrier mobilities in the bilayer structured devices. As shown in Figure

© 2024 Wiley-VCH GmbH

15214095, 2025, 25, Downloaded from https://advanced.onlinelibrary.wiley.com/doi/10.1002/adma.202412239 by Biwu Ma - Florida State University , Wiley Online Library on [20/12/2025]. See the Terms and Conditions (https://onlinelibrary.wiley.com/terms-and-conditions) on Wiley Online Library for rules of use; OA articles are governed by the applicable Creative Commons License

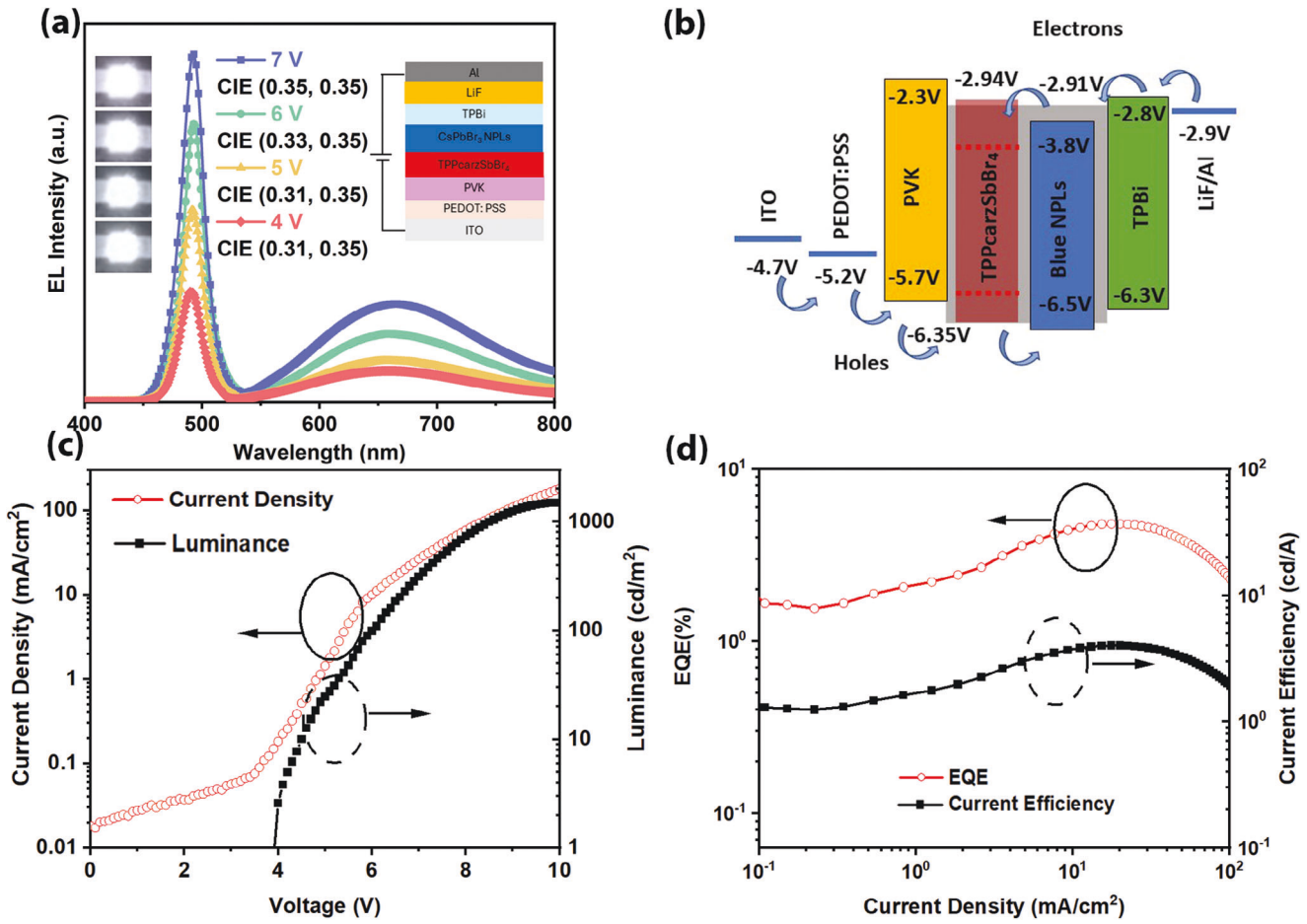

Figure 4. a) EL spectra and corresponding CIE coordinates of 0D $TPPcarzSbBr_4$/2D $CsPbBr_3$ NPLs bilayer structured WLEDs at various driving voltages (the insets show photos of working devices and the device structure). b) Schematic of device operation of bilayer structured WLEDs. c) Current density–voltage–luminance and d) EQE–current density–current efficiency diagrams of a bilayer structured WLED.

S6 (Supporting Information), similar current densities were obtained for single-carrier bilayer structured devices, suggesting balanced hole and electron injections. The hole and electron charge carrier mobilities of bilayer thin films were measured to be 5.5×10^{-6} and 7.0×10^{-6} $cm^2\ V^{-1}\ s^{-1}$ (Figure S7, Supporting Information), suggesting good charge transport of bilayer thin films for device operations. Given the presence of the same wide bandgap semiconducting $TPPcarz^+$ units in both 0D $TPPcarzSbBr_4$ and 2D $CsPbBr_3$ NPLs layers, the emitting bilayer can be viewed as having $TPPcarz^+$ as the host, with antimony bromide anions ($Sb_2Br_8^{2-}$) and $CsPbBr_3$ NPLs serving as the light emitters. In other words, the recombination of charge carriers to form excitons in $TPPcarz^+$ units occur across the bilayer and is subsequently harvested by the emitting species without energy transfer between them. Figure 4b presents the energy alignment for the device, where the band edge values of the charge transport materials, TPPcarzBr/$TPPcarz_2SO_4$, and 2D $CsPbBr_3$ NPLs are referenced from the literature.[14b,17a,24] The large grey region represents the TPPcarzBr and $TPPcarz_2SO_4$ ligands, which serve as host on the surface of 2D $CsPbBr_3$ NPLs and as components of $TPPcarzSbBr_4$. The direct band gap of $TPPcarzSbBr_4$ was determined through UV absorption and cyclic voltammetry (Figure S8, Supporting Information), which is comparable to that of TPPcarzBr/$TPPcarz_2SO_4$. It is important to note that the energy band edge we obtained does not directly correspond to the emission band energy of the red emitter, $Sb_2Br_8^{2-}$, in the $TPPcarzSbBr_4$ layer. The self-trapped emission in $TPPcarzSbBr_4$ is phosphorescence, resulting from the radiative recombination of localized excitons in the $Sb_2Br_8^{2-}$ species, which undergo significant excited-state structural reorganization. Consequently, the actual emission band gap is smaller than the direct band gap calculated from UV absorption and cyclic voltammetry, and dashed lines are used to indicate the red emission gap. Figure 4c,d show the device characteristics of a bilayer structured WLED, which features a low turn-on voltage of 3.9 V, a high luminance of 1507 cd m^{-2} at 9.5 V, an EQE of 4.8%, and a current efficiency of 4.0 cd A^{-1}. The gap between our experimental EQEs and the theoretical EQE limit (20%–30%) can be attributed to several factors. First, the devices showed a reduction in EQE at high current densities, commonly known as efficiency roll-off, a typical issue for most PeLEDs. This indicates that band bending from interfacial effects and variations in dielectric constants across the multilayer structure contribute to non-radiative processes, such as Auger recombination and interface-induced recombination. Additionally,

© 2024 Wiley-VCH GmbH

15214095, 2025, 25, Downloaded from https://advanced.onlinelibrary.wiley.com/doi/10.1002/adma.202412239 by Biwu Ma - Florida State University , Wiley Online Library on [20/12/2025]. See the Terms and Conditions (https://onlinelibrary.wiley.com/terms-and-conditions) on Wiley Online Library for rules of use; OA articles are governed by the applicable Creative Commons License

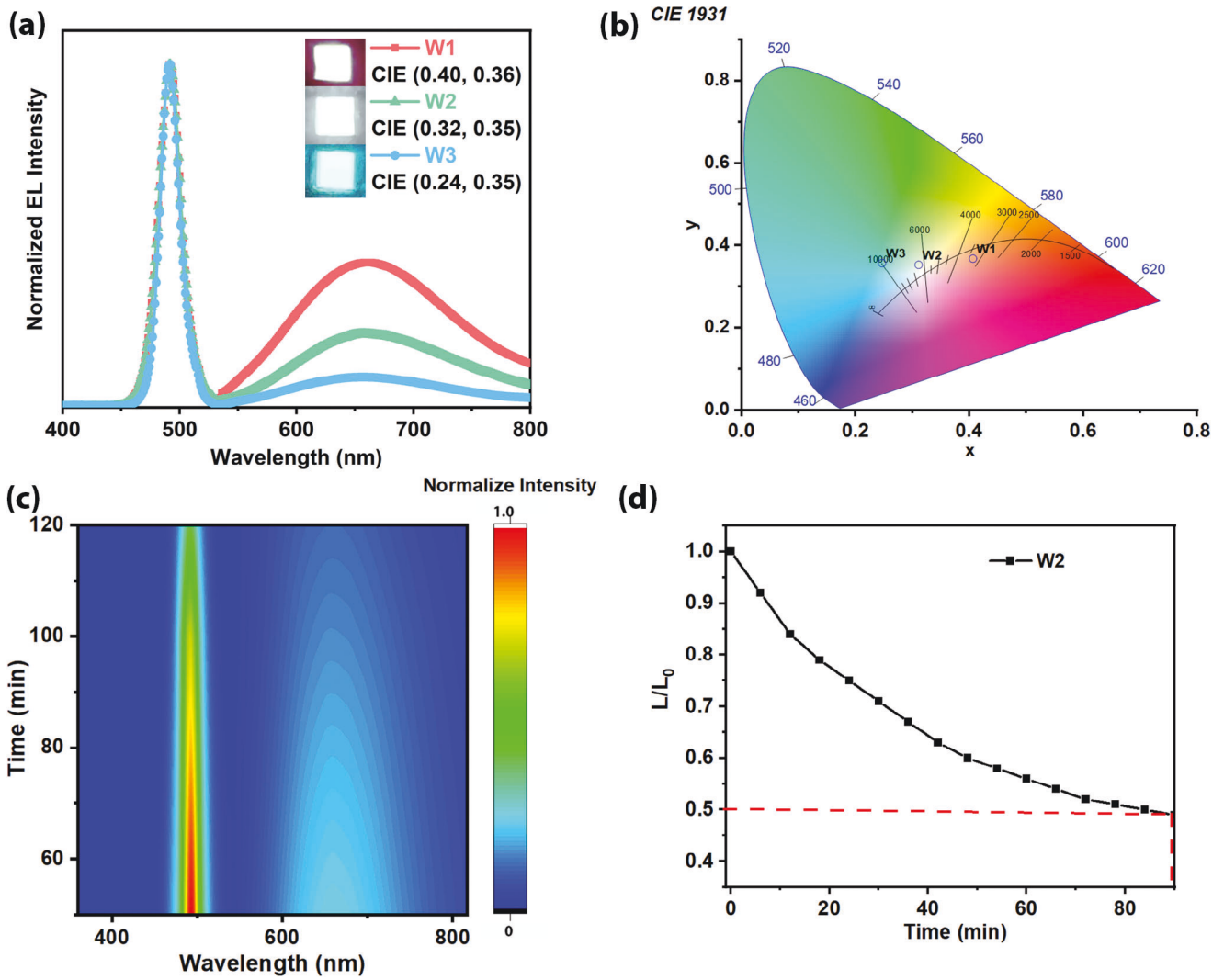

Figure 5. a) EL spectra and b) corresponding CIE coordinates of devices W1, W2, and W3. c) The EL spectra changes with the operational lifetime of the fabricated W2 WLEDs. d) T_{50} of the fabricated W2 WLEDs.

an excess of charge carriers passing through the device without forming electron-hole pairs leads to Joule heating.[25] The electric field distribution within the device was not fully optimized, resulting in incomplete radiative decay of excitons. Consequently, the IQE of the device is lower than the overall PLQE of 79.3% for the bilayer emitting layer. Moreover, 2D $CsPbBr_3$ NPLs exhibit a small Stokes shift with significant overlap between the absorption and emission spectra, resulting in substantial reabsorption of emitted photons, further contributing to EQE losses. Lastly, no strategy was implemented to improve light outcoupling or extraction efficiency in this study. We believe that with careful device engineering, the gap between experimental and theoretical EQEs could be greatly reduced.

To further demonstrate the advantages of our WLEDs based on emitting bilayers without energy transfer, we fabricated devices with various thicknesses of 0D $TPPcarzSbBr_4$ and 2D $CsPbBr_3$ NPLs layers for tunable white emissions. By varying the thickness of 0D $TPPcarzSbBr_4$ layer from 50 to 40 and 30 nm, while keeping the thickness of the layer of 2D $CsPbBr_3$ NPLs at ≈70 nm, we can produce LEDs with warm to cold white emissions (W1–W3) (**Figure** 5a). The CIE coordinate shifts from (0.40, 0.36) for W1 to (0.32, 0.35) for W2 and (0.24, 0.35) for W3 (Figure 5b), while the CCT changes from 3295 to 6502K and 11429K. These results confirm that the charge recombination and exciton harvesting occur across the emitting bilayer, with the two emitting species emitting light independently without influencing each other. Moreover, our device design allows WLEDs to achieve excellent spectral stability and operating lifetime. As shown in Figure 5c,d, both the spectral stability and operating lifetime were tested at an initial brightness of 100 cd m^{-2} under a constant driving current. The EL spectrum remained stable for over 120 min, and the T_{50} for unencapsulated devices was ≈90 min.

3. Conclusion

In summary, we have successfully demonstrated a facile approach for fabricating WLEDs by solution processing emitting bilayers consisting of surface passivated sky blue 2D

© 2024 Wiley-VCH GmbH

15214095, 2025, 25, Downloaded from https://advanced.onlinelibrary.wiley.com/doi/10.1002/adma.202412239 by Biwu Ma - Florida State University , Wiley Online Library on [20/12/2025]. See the Terms and Conditions (https://onlinelibrary.wiley.com/terms-and-conditions) on Wiley Online Library for rules of use; OA articles are governed by the applicable Creative Commons License

$CsPbBr_3$ NPLs and orange/red 0D $TPPcarzSbBr_4$. The unique photophysical properties of 2D $CsPbBr_3$ NPLs and 0D $TPPcarzSbBr_4$ ensure that no energy transfer occurs between them when stacked to form emitting bilayers, due to the absence of spectral overlap. The presence of the same semiconducting organic cation $TPPcarz^+$ in both surface passivated 2D $CsPbBr_3$ NPLs and 0D $TPPcarzSbBr_4$ enables the formation of smooth bilayers with well aligned energy levels and efficient charge transport with $TPPcarz^+$ serving as a common host for both sky blue and orange/red emitting species. We believe that this simple device architecture offers a practical concept for WLED design and paves the way for the further development of high-performance WLEDs utilizing metal halide perovskites and perovskite-related organic metal halide hybrids.

4. Experimental Section

Materials: PEDOT: PSS (4083) was purchased from Heraeus. Antimony(III) bromide, triphenylphosphine (TPP, Aldrich, 99%), 3-bromo-9-phenylcarbazole, poly(N-vinylcarbazole) (PVK), LiF, dichloromethane (99.5%) and diethyl ether (Et2O, anhydrous), Dimethylformamide (DMF, anhydrous), hydrobromic acid (48%), $PbBr_2$, Cs_2CO_3, 1-octadecene (90%), H_2SO_4 (98%), oleylamine (70%), oleic acid (90%), 2-propanol (IPA, anhydrous, 99.5%), octane (anhydrous, 99%), LiF, were purchased from Sigma–Aldrich. Chlorobenzene (anhydrous, 99.8%) and ethylene glycol were purchased from VWR. All reagents and solvents were used without further purification unless otherwise stated.

Synthesis of TPPcarzBr and $TPPcarz_2SO_4$: The TPPcarzBr was synthesized according to the reported method.[26] Triphenylphosphine (524 mg, 2 mmol), 3-bromide-9-phenylcarbazole (644 mg, 2 mmol), and $NiBr_2$ (50 mg, 0.2 mmol) were added in 5 mL of ethylene glycol solution and stirred for 5 h at 150 °C. The resulting deep green solution was then dissolved in water and extracted with CH_2Cl_2. The white powder product was washed with diethyl ether. Yield: 95%. ^{1}H NMR (500 MHz, CDCl3, δ): 8.28-8.22 (d, 1H), 8.10-8.05 (d, 1H), 7.98-7.89 (m, 3H), 7.85-7.78 (m, 6H), 7.74-7.63 (m, 9H), 7.59-7.48 (m, 5H), 7.45-7.41 (d, 1H), 7.39-7.35(t, 1H). $TPPcarz_2SO_4$ was synthesized by mixing TPPcarzBr with an equivalent amount of H_2SO_4 in an ethanol medium, followed by washing with ethyl ether and drying under vacuum.

Synthesis of 2D $CsPbBr_3$ NPLs: 2D $CsPbBr_3$ NPLs were synthesized following modified reported procedures.[18,27] Cs_2CO_3 (0.325 g) and oleic acid (10 mL) were combined in a vial and heated to 120 C until Cs_2CO_3 was fully dissolved, forming a cesium-oleate (CsOA) solution. In a separate vial, $PbBr_2$ (0.073 g), 1-octadecene (4 mL), oleylamine (0.5 mL), oleic acid (0.5 mL), 0.15 mmol $TPPcarz_2SO_4$ and TPPcarzBr were added and heated to 120 °C until $PbBr_2$ was completely dissolved. Next, 0.5 mL of the CsOA solution was injected into the $PbBr_2$ solution at room temperature. After stirring for 30 s, 0.5 mL of IPA was added. The mixture was then heated to 85 °C and maintained for 10 min, before being cooled in an ice water bath. The crude sample was centrifuged at 4 000 rpm. to separate the unreacted precursors.

Purification of Colloidal 2D $CsPbBr_3$ NPLs: The 6 mL of crude sample was combined with 12 mL of toluene and separated by centrifugation at 12 000 rpm. for 5 min. To remove excess organic ligands, the precipitate was dispersed in a mixture of 5 mL toluene and 10 mL methyl acetate, then centrifuged at 4 000 rpm. To remove the supernatant, a process was repeated twice. Finally, the precipitate was resuspended in 2 mL of octane to serve as the emitter layer for LED devices and for material characterizations.

Fabrication of Sky-Blue LEDs Based on 2D $CsPbBr_3$ NPLs: ITO glass substrates were cleaned using a detergent solution, deionized water, acetone, and 2-propanol, followed by treatment with a UV ozone cleaner for 20 min. A 40 nm layer of PEDOT: PSS was spin-coated at 4500 rpm. for 45 s and then baked at 150 °C for 20 min. Next, a 35 nm layer of 4 mg mL^{-1} PVK chlorobenzene solution was spin-coated at 2500 rpm. for 30 s and annealed at 150 °C for 20 min. Following this, a 70 nm emissive NPLs layer was spin-coated in 2 000 rpm. for 30 s. Finally, layers of 40 nm TPBi, 1 nm LiF, and 100 nm Al were sequentially deposited using a thermal evaporator under high vacuum conditions (<2 × 10^−6 mbar). 2D $CsPbBr_3$ NPLs devices designed for hole and electron transport were fabricated with the following structures: Hole-only device: ITO/PEDOT: PSS (40 nm)/2D $CsPbBr_3$ NPLs (70 nm)/MoOx (10 nm)/Al (100 nm). Electron-only device: ITO/SnO_2 (30 nm)/2D $CsPbBr_3$ NPLs (70 nm)/LiF (2 nm)/Al (100 nm).

Fabrication of WLEDs: The WLEDs were fabricated with the configuration of ITO/PEDOT: PSS (40 nm)/PVK (35 nm)/$TPPcarzSbBr_4$ (40 nm)/2D $CsPbBr_3$ NPLs (70 nm)/TPBi (40 nm)/LiF (2 nm)/Al (100 nm). ITO substrates were cleaned by sonication in detergent solution, deionized water, acetone, and 2-propanol, followed by a nitrogen purge and ultraviolet-ozone treatment for 20 min. PEDOT: PSS was spin-coated at 4500 rpm. for 45 s and baked at 150 °C for 20 min. PVK (in chlorobenzene, 4 mg mL^{-1}) was deposited on top at 2500 rpm. for 30 s, followed by drying at 150 °C for 20 min. The 0D $TPPcarzSbBr_4$ layer was deposited by spin coating at 2500 rpm. for 45 s using a precursor solution (0.2 mmol $SbBr_3$ and 0.4 mmol TPPcarzBr in a 1:2 molar ratio in 1 mL DMF) and annealed at 90 °C for 10 min. Subsequently, the 2D $CsPbBr_3$ NPLs solution was spin-coated in 2 000 rpm. for 30 s. Finally, 1 nm of LiF and 100 nm of Al were thermally deposited under a high vacuum of ≈2 × 10^−6 torr. White bilayers devices designed for hole and electron transport were fabricated with the following structures: Hole-only device: ITO/PEDOT: PSS (40 nm)/ $TPPcarzSbBr_4$ (40 nm)/ 2D $CsPbBr_3$ NPLs (70 nm)/MoOx (10 nm)/Al (100 nm). Electron-only device: ITO/SnO_2 (30 nm)/ $TPPcarzSbBr_4$ (40 nm)/ 2D $CsPbBr_3$ NPLs (70 nm)/LiF (2 nm)/Al (100 nm).

Material and Device Characterizations: PL spectra were obtained using an Edinburgh FS5 steady-state spectrometer with a 150 W xenon lamp and 365 nm excitation. And time-resolved PL were measured using the same equipment with a 150 W xenon lamp and excited at 365 nm. The PL decay was fitted with a biexponential decay, and the weighted average lifetime was obtained according to equation $\tau_{ave} = \Sigma\alpha i\tau i^2/\Sigma\alpha i\tau i$, i = 1, 2. Absorption spectra were measured using an Agilent Technologies Cary 5 000 UV–vis–NIR spectrophotometer. PLQEs were recorded with a Quantaurus-QY spectrometer (model Hamamatsu C11347-11), equipped with a 150 W xenon lamp. The PLQE values were calculated using the equation: η_{QE} =, where I_s represents the emission spectra of the samples, E_R represents the spectra of the excitation spectra of the reference (blank substrate), and E_s refers to the excitation spectra of the sample. TEM images were taken on a JEOL JEM-ARM200cF microscope at 200 kV. AFM images were measured using a Bruker Icon scanning probe microscope in tapping mode. The EL spectra were collected using a USB4000 spectrometer. The *J–V–L* characteristics were measured with a Keithley 2400 source meter coupled to a Si photodiode. The charge carrier mobilities are determined from the space-charge-limited current (SCLC) region using the Mott–Gurney equation. The charge-carrier mobility (μ) was determined using Mott–Gurney (M–G) analysis in trap-controlled space-charge limited current (SCLC) region of the *J–V* curves; $\mu = (8JL^3)/(9\varepsilon\varepsilon_0V^2)$, μ is the carrier mobility, where ε_0 is the dielectric constant of vacuum, ε is the dielectric constant of 2D $CsPbBr_3$ NPLs and 0D $TPPcarzSbBr_4$ obtained by the via capacitance measurements.[17] Device measurements were conducted under ambient conditions at room temperature.

Supporting Information

Supporting Information is available from the Wiley Online Library or from the author.

Acknowledgements

The authors thank the support from the National Science Foundation (ECCS-2204466 and ECCS-1912911) and the FSU Office of Research. A portion of this research used resources provided by the X-ray Crystallography Center (FSU075000XRAY) and the Materials Characterization Laboratory (FSU075000MAC) at the FSU Department of Chemistry and

 © 2024 Wiley-VCH GmbH

15214095, 2025, 25, Downloaded from https://advanced.onlinelibrary.wiley.com/doi/10.1002/adma.202412239 by Biwu Ma - Florida State University , Wiley Online Library on [20/12/2025]. See the Terms and Conditions (https://onlinelibrary.wiley.com/terms-and-conditions) on Wiley Online Library for rules of use; OA articles are governed by the applicable Creative Commons License

Biochemistry, as well as the Department of Physics Condensed Matter and Material Physics (CMMP) user facility.

Conflict of Interest

The authors declare no conflict of interest.

Data Availability Statement

The data that support the findings of this study are available in the supplementary material of this article.

Keywords

bilayer structure, light emitting diodes, metal halide perovskites, white emission, 0-D organic metal halide hybrid

Received: August 18, 2024
Revised: October 4, 2024
Published online: November 6, 2024

[1] a) P. Chenna, S. Gandi, S. Pookatt, S. Parne, *Mater. Today. Electron.* **2023**, *5*, 100057; b) J. Ma, R. Yang, Y. Chen, Y. Liu, S. Chen, *Prog. Chem.* **2024**, *36*, 224; c) F. Wang, H. Pan, W. Mao, D. Wang, *Heliyon* **2024**, *10*, e34795.

[2] a) J. Cho, J. H. Park, J. K. Kim, E. F. Schubert, *Laser Photonics Rev.* **2017**, *11*, 1600147; b) M. Worku, L. J. Xu, M. Chaaban, A. Ben-Akacha, B. W. Ma, *APL Mater.* **2020**, *8*, 010902; c) L. Cao, W. Li, B. Devakumar, N. Ma, X. Huang, A. Lee, *ACS Appl. Mater. Interfaces.* **2022**, *14*, 5643.

[3] a) W. Bae, J. Lim, D. Lee, M. Park, H. Lee, J. Kwak, K. Char, C. Lee, S. Lee, *Adv. Mater.* **2014**, *26*, 6387; b) S. Lim, Y. Ko, C. Rodriguez, S. Gong, Y. Cho, *Light-Sci. Appl.* **2016**, *5*, e16030.

[4] a) M. C. Gather, A. Kohnen, K. Meerholz, *Adv. Mater.* **2011**, *23*, 233; b) S. Reineke, M. Thomschke, B. Lussem, K. Leo, *Rev. Mod. Phys.* **2013**, *85*, 1245; c) L. Yang, S. Zhang, B. Xu, J. Jiang, B. Cai, X. Lv, Y. Zou, Z. Fan, H. Yang, H. Zeng, *Nano Lett.* **2023**, *23*, 2443.

[5] a) F. Zhang, J. Song, B. Han, T. Fang, J. Li, H. Zeng, *Small Methods* **2018**, *2*, 1700382; b) Y. Zhang, Z. Zhang, W. Yu, Y. He, Z. Chen, L. Xiao, J. Shi, X. Guo, S. Wang, B. Qu, *Adv. Sci.* **2022**, *9*, 2102895.

[6] a) L. N. Quan, B. P. Rand, R. H. Friend, S. G. Mhaisalkar, T. W. Lee, E. H. Sargent, *Chem. Rev.* **2019**, *119*, 7444; b) Z. K. Tan, R. S. Moghaddam, M. L. Lai, P. Docampo, R. Higler, F. Deschler, M. Price, A. Sadhanala, L. M. Pazos, D. Credgington, F. Hanusch, T. Bein, H. J. Snaith, R. H. Friend, *Nat. Nanotechnol.* **2014**, *9*, 687.

[7] a) Z. Liu, W. D. Qiu, X. M. Peng, G. W. Sun, X. Y. Liu, D. H. Liu, Z. C. Li, F. R. He, C. Y. Shen, Q. Gu, F. L. Ma, L. Yip, L. T. Hou, Z. J. Qi, S. J. Su, *Adv. Mater.* **2021**, *33*, 2103268; b) Q. Wan, W. L. Zheng, C. Zou, F. Carulli, C. Y. Zhang, M. M. Liu, Q. G. Zhang, L. Kong, H. L. Song, L. Y. Lin, L. Li, S. Brovelli, *ACS Energy. Lett.* **2023**, *8*, 927; c) J. Jiang, Z. M. Chu, Z. G. Yin, J. Z. Li, Y. G. Yang, J. R. Chen, J. L. Wu, J. B. You, X. W. Zhang, *Adv. Mater.* **2022**, *34*, 2204460; d) M. Worku, A. Ben-Akacha, T. B. Shonde, H. Liu, B. W. Ma, *Small Science* **2021**, *1*, 2000072; e) X. R. Chen, H. Y. Xiang, R. Wang, Y. F. Wang, Y. J. Wang, H. B. Zeng, *Adv. Funct. Mater.* **2023**, *33*, 2304750; f) D. Yan, S. Zhao, Y. Zhang, H. Wang, Z. Zang, *Opto-Electron. Adv.* **2022**, *5*, 200075; g) S. Chen, J. Lin, S. Zheng, Y. Zheng, D. Chen, *Adv. Funct. Mater.* **2023**, *33*, 2213442.

[8] S. Q. Sun, Y. T. Cai, M. Zhu, W. He, B. C. Liu, Y. L. Xu, X. Lv, Q. Sun, P. Y. Liu, T. T. Shi, Y. M. Xie, M. K. Fung, *Adv. Funct. Mater.* **2023**, *33*, 2306549.

[9] a) R. Wang, H. Y. Xiang, Y. Li, Y. H. Zhou, Q. S. Shan, Y. Q. Su, Z. Li, Y. J. Wang, H. B. Zeng, *Adv. Funct. Mater.* **2023**, *33*, 2215189; b) W. D. Sun, S. J. Jiao, S. B. Li, D. Y. Zhang, X. Y. Xia, L. Zhou, *Adv. Opt. Mater.* **2023**, *11*, 2300902.

[10] Y. Xie, L. Liao, M. Fung, *Adv. Funct. Mater.* **2024**, 2401789.

[11] a) Z. Q. Guan, Y. Li, Z. H. Zhu, Z. X. Zeng, D. Shen, J. H. Tan, S. W. Tsang, S. A. Liu, C. S. Lee, *ACS Appl. Mater. Interfaces.* **2021**, *13*, 44991; b) D. H. Liu, X. Y. Liu, Y. Y. Gan, Z. Liu, G. W. Sun, C. Y. Shen, X. M. Peng, W. D. Qiu, D. L. Li, Z. S. Zhou, Z. C. Li, H. L. Yip, S. J. Su, *ACS Energy. Lett.* **2022**, *7*, 523.

[12] D. Das, P. Gopikrishna, D. Barman, R. Yathirajula, P. Iyer, *Nano Convergence* **2019**, *6*, 31.

[13] G. Nair, H. Swart, S. Dhoble, *Prog. Mater. Sci.* **2020**, *109*, 100622.

[14] a) J. Li, Y. Sang, L. Xu, H. Lu, J. Wang, Z. Chen, *Angew. Chem.-Int. Ed.* **2022**, *61*, e202113450; b) R. L. Z. Hoye, M. L. Lai, M. Anaya, Y. Tong, K. Galkowski, T. Doherty, W. W. Li, T. N. Huq, S. Mackowski, L. Polavarapu, J. Feldmann, J. L. MacManus-Driscoll, R. H. Friend, A. S. Urban, S. D. Stranks, *ACS Energy. Lett.* **2019**, *4*, 1181.

[15] M. Worku, Y. Tian, C. K. Zhou, S. Lee, Q. Meisner, Y. Zhou, B. W. Ma, *ACS Appl. Mater. Interfaces.* **2018**, *10*, 30051.

[16] C. K. Zhou, H. R. Lin, Q. Q. He, L. J. Xu, M. Worku, M. Chaaban, S. Lee, X. Q. Shi, M. H. Du, B. W. Ma, *Mater. Sci. Eng. R-Rep.* **2019**, *137*, 38.

[17] a) H. Liu, T. B. Shonde, F. Gonzalez, O. J. Olasupo, S. J. Lee, D. Luong, X. S. Lin, J. Winfred, E. Lochner, I. Fatima, K. Hanson, B. W. Ma, *Adv. Mater.* **2023**, *35*, 2209417; b) H. Liu, T. B. Shonde, O. J. Olasupo, M. S. Islam, T. F. Manny, M. Woodhouse, X. S. Lin, J. Winfred, K. S. Mao, E. Lochner, I. Fatima, K. Hanson, B. W. Ma, *ACS Energy Lett.* **2023**, *8*, 4259.

[18] J. Shamsi, P. Rastogi, V. Caligiuri, A. L. Abdelhady, D. Spirito, L. Manna, R. Krahne, *ACS Nano* **2017**, *11*, 10206.

[19] Y. Bekenstein, B. A. Koscher, S. W. Eaton, P. D. Yang, A. P. Alivisatos, *J. Am. Chem. Soc.* **2015**, *137*, 16008.

[20] S. Park, J. E. Kwon, S. H. Kim, J. Seo, K. Chung, S.-Y. Park, D.-J. Jang, B. M. Medina, J. Gierschner, S. Y. Park, *J. Am. Chem. Soc.* **2009**, *131*, 14043.

[21] a) S. Riera-Galindo, A. Tamayo, M. Mas-Torrent, *ACS Omega* **2018**, *3*, 2329; b) P. Kundu, K. Thomas, J. Lin, Y. Tao, C. Chien, *Adv. Funct. Mater.* **2003**, *13*, 445.

[22] H. Liu, M. Worku, A. Mondal, T. Shonde, M. Chaaban, A. Ben-Akacha, S. Lee, F. Gonzalez, O. Olasupo, X. Lin, J. Winfred, Y. Xin, E. Lochner, B. Ma, *Adv. Energy. Mater.* **2023**, *13*, 2201605.

[23] M. Worku, A. Ben-Akacha, S. Sridhar, J. Frick, S. Yin, Q. He, A. Robb, M. Chaaban, H. Liu, J. Winfred, K. Hanson, F. So, D. Dougherty, B. Ma, *Adv. Funct. Mater.* **2021**, *31*, 2103299.

[24] Z. Zhu, Y. Wu, Y. Shen, J. Tan, D. Shen, M. Lo, M. Li, Y. Yuan, J. Tang, W. Zhang, S. Tsang, Z. Guan, C. Lee, *Chem. Mater.* **2021**, *33*, 4154.

[25] W. Zou, R. Li, S. Zhang, Y. Liu, N. Wang, Y. Cao, Y. Miao, M. Xu, Q. Guo, D. Di, L. Zhang, C. Yi, F. Gao, R. Friend, J. Wang, W. Huang, *Nat. Commun.* **2018**, *9*, 608.

[26] L.-J. Xu, M. Worku, Q. He, H. Lin, C. Zhou, B. Chen, X. Lin, Y. Xin, B. Ma, *J. Phys. Chem. Lett.* **2019**, *10*, 5836.

[27] J. Shamsi, D. Kubicki, M. Anaya, Y. Liu, K. Ji, K. Frohna, C. P. Grey, R. H. Friend, S. D. Stranks, *ACS Energy. Lett.* **2020**, *5*, 1900.

© 2024 Wiley-VCH GmbH

15214095, 2025, 25, Downloaded from https://advanced.onlinelibrary.wiley.com/doi/10.1002/adma.202412239 by Biwu Ma - Florida State University , Wiley Online Library on [20/12/2025]. See the Terms and Conditions (https://onlinelibrary.wiley.com/terms-and-conditions) on Wiley Online Library for rules of use; OA articles are governed by the applicable Creative Commons License